

## Implementation of a Software Phantom for the Assessment of Contrast Detail in Digital Radiography

Meletis Liaskos<sup>2</sup>, Christos Michail<sup>1</sup>, Nektarios Kalyvas<sup>2</sup>, Adrianos Toutountzis<sup>1</sup>, Stavros Tsantis<sup>2</sup>, George Fountos<sup>2</sup>, Dionysis Cavouras<sup>2</sup> and Ioannis Kandarakis<sup>2\*</sup>

<sup>1</sup> Department of Medical Physics, Medical School University of Patras 265 00 Patras, Greece

<sup>2</sup> Department of Medical Instruments Technology Technological Educational Institution of Athens Ag. Spyridonos, Aigaleo, 122 10 Athens, Greece

Corresponding author: [kandarakis@teiath.gr](mailto:kandarakis@teiath.gr)

**Abstract.** *The aim of the present study is to simulate a commercial contrast detail phantom - (CDRAD 2.0 phantom) used in the evaluation of both digital and analog radiographic units. This phantom is suitable for the estimation of low contrast resolution. The software phantom was developed in the Matlab 7.01 platform. The results of the software phantom were evaluated with the ones obtained on a digital radiographic unit (DIAGNOST Philips Medical Systems) and showed a very good agreement. The software phantom uses tabulated data for the X-ray spectra and attenuation coefficients in order to simulate the CDRAD images as well as the contrast details versus X-ray energy and phantom depth. This software phantom provides an easy, fast and reliable method for the evaluation of contrast detail in radiographic units (both digital and analog) with the use of a personal computer.*

**Keywords:** Software Phantom, Contrast detail analysis, Digital Radiography.

## 1 INTRODUCTION

The performance of some direct and indirect flat panel detectors (FPD) systems for general radiography has been previously studied, focusing mostly on the comparison of a single FPD with more traditional detectors (SF or CR). Prior studies were based on evaluating physical image quality parameters such as modulation transfer function (MTF), noise power spectrum (NPS), and detective quantum efficiency (DQE), [1],[2] psychophysical tests like contrast detail (CD) analysis, [3]-[5] or both in the context of an observer perception model [6],[7]. Ideally, a complete performance evaluation of the systems should include both physical and psychophysical evaluations under in the same standard conditions. Computer simulations have proven to be valuable tools for experimental investigations, involving radiological exposures and complex phantoms [8]-[12], as they can provide a lot of flexibility and efficiency in setting up controlled experiments. Such simulators are usually application specific and most often are built in-house to meet the specific requirements of the conducted investigation. Several simulators have been reported to address particular image quality studies [8], [13]-[15] that establish critical factors for designing and optimizing imaging systems. Other simulators are dedicated to investigations involving studies of physical events like particle interaction processes and transport [16],[17]. Simulators are also widely used to simulate imaging techniques and to generate sets of image data. Several of these simulators are applied for designing and evaluating innovative imaging techniques and prototype imaging systems [18], [19]. In this study a custom made software was

developed to simulate a commercial contrast detail phantom - (CDRAD 2.0 phantom), compared with experimental results obtained with the CDRAD 2.0 phantom on a FPD system (DIAGNOST Philips Medical Systems) with standard exposure conditions [20,21]. CD curves of the systems were obtained and the experimental CD curves of the systems were compared with the simulated data extended to softcopy image evaluations [22].

According to our knowledge such a study has never been previously carried out for this phantom, which is suitable for the estimation of low contrast resolution. The software phantom was developed in the Matlab 7.01 platform. The results of the software phantom were evaluated with the ones obtained on a digital radiographic unit (DIAGNOST Philips Medical Systems) and showed a very good agreement. The software phantom uses tabulated data for the X-ray spectra and attenuation coefficients in order to simulate the CDRAD images as well as the contrast details versus X-ray energy and phantom depth. This software phantom provides an easy, fast and reliable method for the evaluation of contrast detail in radiographic units (both digital and analog) with the use of a personal computer.

## 2 MATERIALS AND METHODS

### 2.1. Experimental procedure

Matlab 7.01 platform was used in order to simulate images of the CDRAD phantom obtained by a digital X-ray Radiographic unit. Images were obtained for X-ray spectra corresponding to 60 and 125 kV respectively [23]. Digital images of the CDRAD phantom were obtained by exposing the phantom to X-rays on digital radiographic unit (DIAGNOST Philips Medical Systems). The source to detector distance (SDD) was set to: 1.80 m. Automatic exposure control (AEC) was used to obtain the CDRAD images. The X-ray tube had 0.1mm Cu and 1mm Al inherent filtration. The pixel spacing of the FPD was: 0.143X0.143 mm. The Flat-Panel was 43x43 cm. The digital image dimensions were (2969X2945) pixels, with resolution 6.993 pixels per mm and 16 bits per pixel (unsigned short).

### 2.2. Contrast-Detail Phantom Description.

The CDRAD phantom consists of a Plexiglas tablet (square 265X265 mm) with a thickness of 10 mm. The tablet contains cylindrical holes of exact diameter and depth (tolerances: 0.03 mm). The size and depth of the holes are vary logarithmically within 0.32 to 8.00 mm±0.02 mm range along the phantom's structured rows and columns (table 1).

Column	Depth [mm]	Row	Diameter [mm]
1	0.3	1	0.3
2	0.4	2	0.4
3	0.5	3	0.5
4	0.6	4	0.6
5	0.8	5	0.8
6	1.0	6	1.0
7	1.3	7	1.3

8	1.6	8	1.6
9	2.0	9	2.0
10	2.5	10	2.5
11	3.2	11	3.2
12	4.0	12	4.0
13	5.0	13	5.0
14	6.3	14	6.3
15	8.0	15	8.0

Table 1: Depth and diameter of the holes within the phantom

In this phantom, the contrast varies very slowly between adjacent details of the same size. The ratio between a target depth and its adjacent target at lower depth is 2 until 1/3 mm. The small attenuation produced by the targets implies a linear relationship between the targets' depth and contrasts as discussed below so that both the depth and the contrast are reduced to half of their initial values every three target steps. In the tablet a line pattern has been engraved, which was treated with lead-containing paint. The X-ray image will show 255 squares arranged in 15 columns and 15 rows. In each square either only one or two spots are present, being the images of the holes. The first three rows show only one spot, while the other rows have two identical spots in each square, one in the middle and one in a randomly chosen corner, to allow verification of the detection of each object. Easily recognisable patterns have been avoided. Figure 1 shows a schematic representation of the phantom <sup>[24],[25]</sup>.

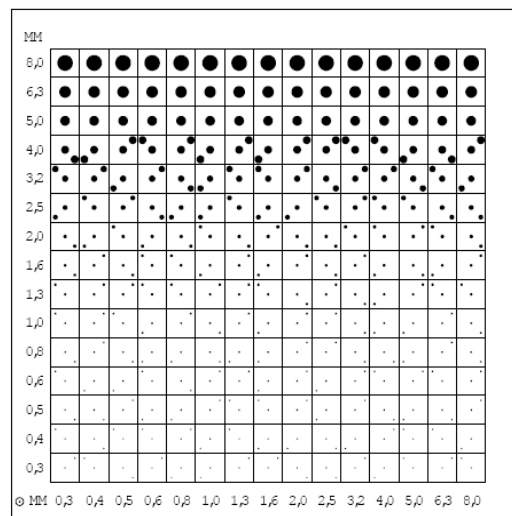


Figure 1 Schematic representation of the CDRAD-phantom.

### 2.3. Process of simulation

The spectrum  $\phi(E)$  of a tungsten anode X-ray tube with no filtering may be given by the following relation <sup>[23]</sup>:

$$\phi(E) = \alpha_0[E] + \alpha_1[E]kVp + \alpha_2[E]kVp^2 + \alpha_3[E]kVp^3 \quad \text{for } E \leq kVp$$

$$\phi(E) = 0 \quad \text{for } E > kVp \quad (1)$$

The predetermined coefficients ( $\alpha_i(E)$ ) are derived from measured data which are necessary to reconstruct the X-ray spectra at any kVp<sup>[23]</sup>. To compute the attenuated spectrum  $\phi_0(E)$  of X-ray beam caused by filters used in the experimental setup, the exponential law was used:

$$\phi_0(E) = \phi(E)e^{-(\mu_{tot,i}(E)/\rho)w} \quad (2)$$

where  $\phi(E)$  is the X-ray spectrum with no filtering computed by relation (1),  $\mu_{tot,i}(E)/\rho$  is the mass attenuation coefficient of the filter, and  $w$  is the thickness of the filter in  $\text{mg}/\text{cm}^2$ <sup>[26]</sup>.  $\phi_0(E)$  is the X-ray photon fluence (photons per unit of area) incident on the scintillator.

Image contrast was evaluated according to equation (3)<sup>[21]</sup>:

$$con = \frac{GLplex - GLhole}{GLhole + GLplex} \quad (3)$$

$GLhole$  and  $GLplex$  represents grey level values in each hole and the adjacent height of Perspex in the phantom respectively.

### 3 RESULTS AND DISCUSSION

Figure 2 shows a CDRAD image obtained experimentally from the DIAGNOST Philips Medical digital X-ray System at 60 kV with exposure time 7.49 ms. In this image we can observe the gray level differentiation from hole to hole. The hole with depth of 8.0 mm is more distinguishable than those of medium or minimum whole depths (e.g. 0.3 mm). Higher contrast can be observed for columns 8 to 15.

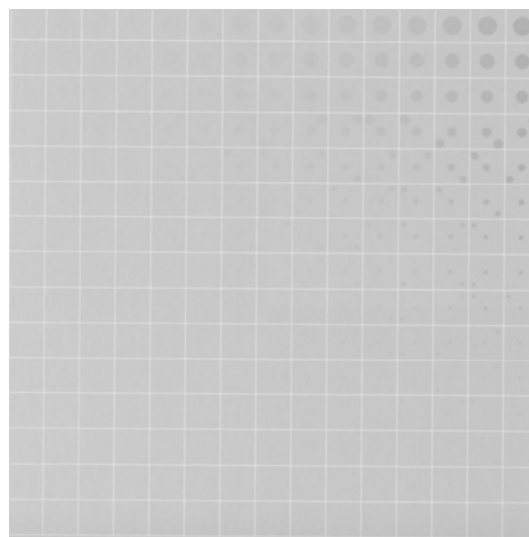


Figure 2: CDRAD image obtained experimentally from the DIAGNOST Philips Medical digital X-ray unit at 60 kV.

Figure 3 shows the simulated image of CDRAD phantom obtained from the custom-made software corresponding to an X-ray spectrum of 60 kV. Figure 3 appears darker than figure 2 due to the normalization in the gray levels, however the resolved wholes are exactly the same as in figure 2. This can be also shown in figure 4 where the contrast detail curves of the simulated and experimentally obtained images are almost the same. The left part of figure 3 shows low depths corresponding to low contrast (about 0 at 0.3 mm) and the right part shows high depths corresponding to high contrast (about 0.14 at 8.0 mm).

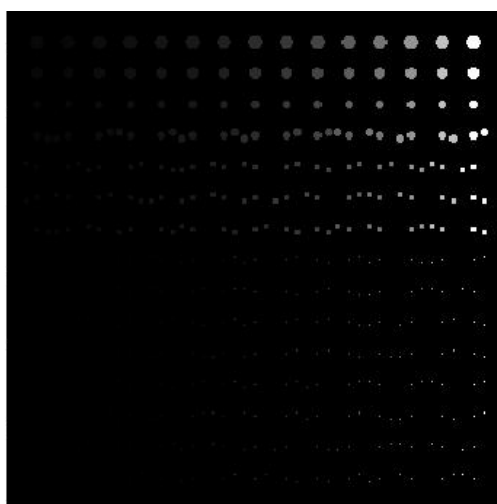


Figure 3: Simulated CDRAD image obtained from the custom-made software corresponding to an X-ray spectrum of 60 kV.

Figure 4 shows contrast detail curves corresponding to the images obtained from the custom-made software and the digital X-ray unit. The simulated curve shows a linear contrast behaviour (due to the assumption of an almost ideal detector) for the various depth values. Almost the same behaviour is shown for the experimentally obtained CDRAD curve. The two curves have a satisfactory correlation coefficient ( $R^2$ ). Contrast for the simulated curve varies from 0.0, for a depth of 0.3mm, to 0.14 for a depth of 8.0 mm. Almost the same values were obtained for the experimentally obtained curve.

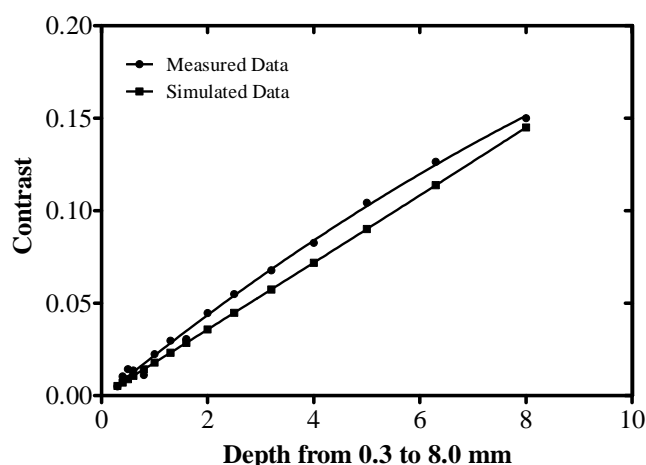


Figure 4: Contrast detail curves corresponding to the image obtained from the custom-made software and the digital X-ray unit for 60 kV.

Figure 5 shows a CDRAD image obtained experimentally from the DIAGNOST Philips Medical digital X-ray System at 125 kV. Exposure time was 1.48 ms. In this image we can observe the gray level differentiation from hole to hole. The hole with depth of 8.0 mm is more distinguishable than those of medium or minimum whole depths (e.g. 0.3 mm). Higher contrast can be observed for columns 10 to 15. In this figure we can see fewer points than figure 2, due to contrast degradation caused by the higher X-ray spectrum (i.e. 125 kV).

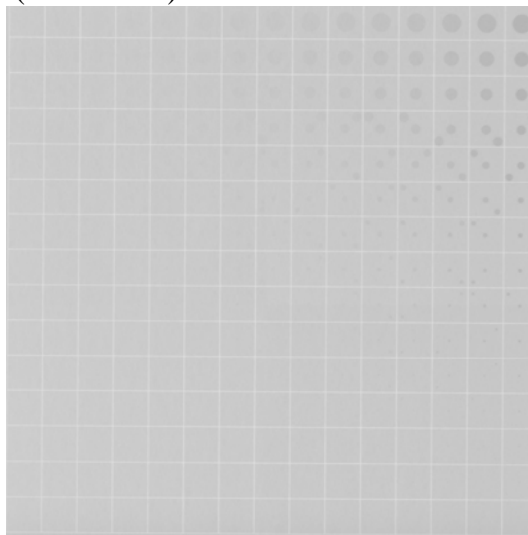


Figure 5: CDRAD image obtained experimentally from the DIAGNOST Philips Medical digital X-ray unit at 125 kV.

Figure 6 shows the simulated image of CDRAD phantom obtained from the custom-made software corresponding to an X-ray spectrum of 125 kV. Figure 6 appears darker than figure 5 due to the normalization in the gray levels, however the resolved wholes are exactly the same as in figure 5. This can be also shown in figure 7 where the contrast detail curves of the simulated and experimentally obtained images are almost the same. The left part of figure 6 shows low depths corresponding to low contrast (about 0 at 0.3 mm) and the right part shows high depths corresponding to high contrast (about 0.12 at 8.0 mm).

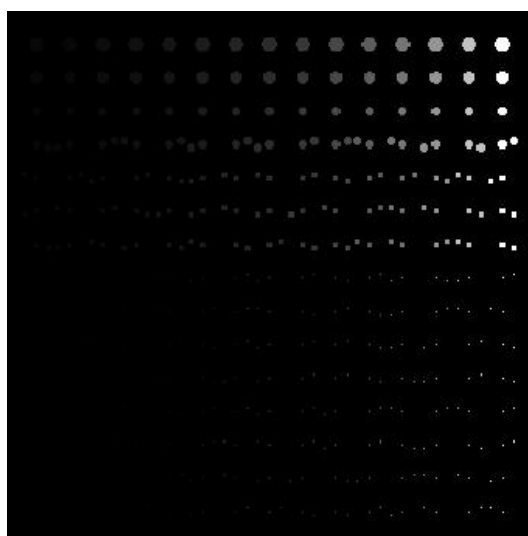


Figure 6: Simulated CDRAD image obtained from the custom-made software corresponding to an X-ray spectrum of 125 kV.

Figure 7 shows contrast detail curves corresponding to the images obtained from the custom-made software and the digital X-ray unit. The simulated graph shows a linear contrast behaviour for the various depth values. Almost the same behaviour is shown for the experimentally obtained CDRAD curve. The two curves have a satisfactory correlation coefficient ( $R^2$ ). Contrast for the simulated curve varies from 0.0, for a depth of 0.3mm, to 0.12 for a depth of 8.0 mm. Almost the same values was obtained for the experimentally obtained curve.

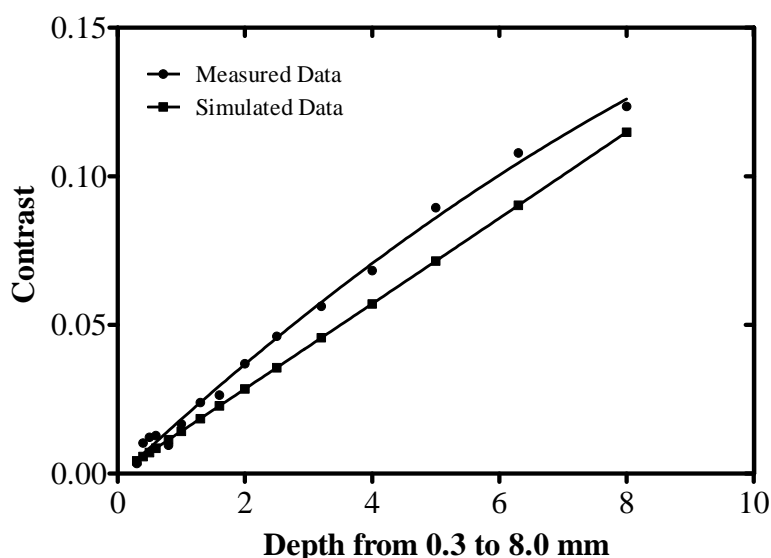


Figure 7: Contrast detail curves corresponding to the image obtained from the custom-made software and the digital X-ray unit for 125 kV.

#### 4 CONCLUSIONS

In this study a custom made software was developed to simulate a commercial contrast detail phantom - (CDRAD 2.0 phantom), evaluated with experimental results obtained with the CDRAD 2.0 phantom on a flat panel detector system (DIAGNOST Philips Medical Systems) with standard exposure conditions. Contrast detail curves of the systems were obtained and the experimental contrast detail curves of the systems were compared with the simulated data extended to softcopy image evaluations. Simulated contrast detail curves showed a very good correlation with the experimental ones at various X-ray set-ups. These findings show that the custom-made software can be used for the evaluation of flat panel detector systems.

#### Acknowledgments

This work is funded by the Greek State Scholarships Foundation (I.K.Y.).

#### REFERENCES

- [1] Granfors P. R, Aufrichtig R. (2000), "Performance of a 41X41-cm<sup>2</sup> amorphous silicon flat panel x-ray detector for radiographic imaging applications," *Med. Phys.* 27, 1324–1331.

- [2] Floyd CE J. R, Warp R. J, J. Dobbins III, Chotas H. G, Baydush A. H, Vargas-Voracek R, Ravin C. E. (2001), "Imaging characteristics of an amorphous silicon flat-panel detector for digital chest radiography," *Radiology* 218, 683–688.
- [3] Chotas H. G, Ravin C. E. (2001), "Digital chest radiography with a solidstate flat-panel x-ray detector: contrast-detail evaluation with processed images printed on film hard copy," *Radiology* 218, 679–682.
- [4] Rong X. J, Shaw C. C, Liu X, Lemacks M. R, Thompson S. K (2001), "Comparison of an amorphous silicon/cesium iodide flat-panel digital chest radiography system with screen/film and computed radiography systems—a contrast-detail phantom study," *Med. Phys.* 28, 2328–2335.
- [5] M. Uffmann, C. Schaefer-Prokop, U. Neitzel, M. Weber, C. J. Herold, and M. Prokop (2004), "Skeletal applications for flat-panel versus storage-phosphor radiography: Effect of exposure on detection of low-contrast details," *Radiology* 231, 506–514.
- [6] Aufrichtig R. (1999), "Comparison of low contrast detectability between a digital amorphous silicon and a screen-film based imaging system for thoracic radiography," *Med. Phys.* 26, 1349–1358.
- [7] R. Aufrichtig, P. Xue (2000), "Dose efficiency and low-contrast detectability of an amorphous silicon x-ray detector for digital radiography," *Phys. Med. Biol.* 45, 2653–2669.
- [8] Sandborg M, Dance D R, Persliden J and Carlsson G A 1994 A Monte Carlo program for the calculation of contrast, noise and absorbed dose in diagnostic radiology *Comput. Methods Programs Biomed.* 42 167–80.
- [9] Morioka C A, Abbey C K, Eckstein M, Close R A, Whiting J S and LeFree M (2000) "Simulating coronary arteries in x-ray angiograms" *Med. Phys.* 27 2438–44.
- [10] Peplow D E, Verghese K (2000), "Digital mammography image simulation using Monte Carlo" *Med. Phys.* 27 568–79.
- [11] Inanc F (2002), "A CT image based deterministic approach to dosimetry and radiography simulations *Phys*". *Med.Biol.* 47 3351–68
- [12] Lazos D, Bliznakova K, Kolitsi Z and Pallikarakis N (2003), "An integrated research tool for x-ray imaging simulation *Comput*". *Methods Programs Biomed.* 70 241–51
- [13] Chan H P, Doi K (1984a) "Studies of x-ray energy absorption and quantum noise properties of x-ray screens by use of Monte Carlo simulation" *Med. Phys.* 11 37–46
- [14] Chan H P, Doi K (1984b) "Radiation dose in diagnostic radiology: Monte Carlo simulation studies *Med*". *Phys.* 11 480–90
- [15] Tapiovaara M J, Sandborg M (1995), "Evaluation of image quality in fluoroscopy by measurements and Monte Carlo calculations *Phys*". *Med. Biol.* 40 589–607
- [16] Persliden J (1983), "A Monte Carlo program for photon transport using analogue sampling of scattering angle in coherent and incoherent scattering processes *Comput*". *Methods Programs Biomed.* 17 115–28
- [17] Freud N, Duvauchelle P, Pistrucci-Maximean S A, L'etang J M and Babot D (2004), "Deterministic simulation of first-order scattering in virtual x-ray imaging *Nucl*". *Instrum. Methods Phys. Res. B* 222 285–300
- [18] Giersch J, Weidemann A, Anton G (2003), "ROSI—an object-oriented and parallel-computing Monte Carlo simulation for x-ray imaging *Nucl*". *Instrum. Methods Phys. Res. A* 509 151–6

- [19] Spyrou G, Panayiotakis G, Tzanakos G (2000), “MASTOS: Mammography simulation tool for design optimization studies Med”. *Inform. Internet. Med.* 25 275–93
- [20] Samei E, Flynn M. J (2003), “An experimental comparison of detector performance for direct and indirect digital radiography systems,” *Med.Phys.* 30, 608–622.
- [21] Borasi G, Samei E, Bertolini M, Nitrosi A, Tassoni D (2006) “Contrast-detail analysis of three flat panel detectors for digital radiography”. *Med. Phys.* 33 6,2006.
- [22] Chan H, Metz C, Doi K (1985), “Digital image processing: optimal spatial filter for maximization of the perceived SNR based on a statistical decision theory model for the human observer.,” *Proc. SPIE* 535, 2–11.
- [23] Boone J.M, Seibert J.A. (1997), “An Accurate Method for Computer Generating Tungsten Anode X-ray spectra from 30kV to 140kV”. *Medical Physics* 24:1661-1670.
- [24] Manual Contrast-Detail Phantom (Artinis Cdrad Type 2.0).
- [25] Aufrechtig R, Xue P (2000), “Dose efficiency and low-contrast detectability of an amorphous silicon x-ray detector for digital radiography”. *Phys. Med. Biol.* 45 2653–2669.
- [26] Boone JM, (2000), “X-ray production, interaction, and detection in diagnostic imaging in *Handbook of Medical Imaging*”. Beutel J, Kundel H L and Van Metter R L, SPIE Press Bellingham.